JOURNAL OF GEOPHYSICAL RESEARCH, VOL. 104, NO. A6, PAGES 12,327–12,337, JUNE 1, 1999

Modeling of time-evolving magnetic fields during substorms

G. Lu,[1] N. A. Tsyganenko,[2] A. T. Y. Lui,[3] H. J. Singer,[4] T. Nagai,[5] and S. Kokubun[6]

Abstract. An attempt has been made to model the dynamics of the magnetospheric magnetic field during substorms by modifying the 1996 version of the data-based model by *Tsyganenko* [1996]. The modified model incorporates an adjustment to the intensity and thickness of the near-tail current sheet and a contribution from the substorm current wedge. These improvements make it possible to use the model to represent the evolution of the magnetic field during the entire substorm sequence of growth, expansion, and recovery. The modeled magnetic fields have been compared to satellite observations during three isolated substorms. According to the model results, during the substorm growth phase the thickness of the tail current sheet was gradually decreased while the intensity of the tail current was gradually increased; by the end of the growth phase a thin current sheet of 190–1340 km in half thickness was formed in a narrow region around $X \sim$ -7.5 R_E, with a maximum westward current density of 9–23 nA/m^2. During the substorm expansion phase an eastward current associated with the substorm current wedge started to develop around $X \sim$ -12 R_E, resulting in a collapse of the previously stretched field configuration. At the peak of an intense substorm the net tail current flow became eastward between $X =$ -11 and $X =$ -13 R_E, accompanied by a negative (southward) B_z tailward of -13 R_E.

1. Introduction

There currently exist several magnetospheric magnetic field models. Among them, a series of data-based empirical models [i.e., *Tsyganenko*, 1987, 1989, 1995, 1996] (hereinafter referred to as T87, T89, T95, and T96, respectively) has been widely used. These models are based on statistical analysis of many years of satellite observations and are quasi-steady in nature. Therefore they are not suitable for studying time-varying phenomena such as substorms. Efforts in developing a time-dependent magnetic field model have been made by *Pulkkinen et al.* [1991, 1992, 1994, 1998]. However, their approach was based on the T89 model, which did not have a realistic magnetopause and which did not include explicitly the field-aligned current system. T89 was parameterized only by means of binning data into several intervals according to the 3-hour *Kp* index and did not include large-scale effects of the solar wind conditions upon the geomagnetic field configuration. In their studies, Pulkkinen et al. modified the intensity and thickness of the tail current in order to model the stretching of the magnetic field during the substorm growth phase and the relaxation during the recovery phase. Because of the lack of the substorm wedge currents, their model could not replicate the substorm expansion phase. So far, the modeling studies of Pulkkinen et al. have been the only effort to empirically represent the substorm growth and recovery phases [*Pulkkinen et al.*, 1991, 1992, 1994, 1995, 1998].

In this paper, we introduce an improved time-evolving magnetic field model, aimed at representing temporal variations of the magnetospheric currents during a substorm. Our study is based on the T96 model, with modifications to the intensity and thickness of the tail currents [*Tsyganenko and Peredo*, 1994], along with an additional magnetic field due to the substorm wedge currents [*Tsyganenko*, 1997]. The main feature of this new time-evolving model is that it can be applied to study the entire substorm process, including the growth, the expansion, and the recovery phase.

2. Model Description

As described by *Tsyganenko* [1996], the T96 model has been improved over its predecessors in several aspects. The total field in T96 is the sum of contributions from all major magnetospheric currents, including the

[1] High Altitude Observatory, National Center for Atmospheric Research, Boulder, Colorado.

[2] Raytheon STX Corporation, Greenbelt, Maryland.

[3] Applied Physics Laboratory, Johns Hopkins University, Laurel, Maryland.

[4] Space Environment Center, National Oceanic and Atmospheric Administration, Boulder, Colorado.

[5] Tokyo Institute of Technology, Tokyo, Japan.

[6] Solar-Terrestrial Environment Laboratory, Nagoya University, Nagoya, Japan.

Paper number 1999JA900145.
0148-0227/99/1999JA900145$09.00

ring current, the tail current, and the region 1 and region 2 field-aligned currents, plus the interconnection field due to partial penetration of the interplanetary magnetic field (IMF). The shielding fields for each magnetospheric current system are introduced separately to ensure a proper confinement of the total field within the magnetopause for any specific combination of the input parameters. The model is parameterized by the solar wind dynamic pressure, the IMF B_y and B_z components, and the *Dst* index.

In the T96 model, the total magnetic field of the cross-tail current was represented as a sum of two independent modules for the two current sheets with essentially different variations of the current density along the tail [*Tsyganenko and Peredo*, 1994; *Tsyganenko*, 1995, 1996]. In the first module the current density rapidly increased at the inner edge of the current sheet located at X = -4 R_E, peaked at X = -10 R_E, and then gradually fell off to zero at larger tailward distances. The second module was introduced in order to maintain the correct values of the magnetic field in the distant magnetotail. The strength of the current in that module was smoothly increased from zero at X = -10 R_E to a finite asymptotic value, providing a magnetic field of $\sim$ 10 nT at and beyond lunar orbit, in accordance with ISEE 3 [e.g., *Slavin et al.*, 1985] and Geotail [*Yamamoto et al.*, 1994] observations. The amplitude of the total current in the two modules was parameterized by the solar wind pressure and by the IMF, and they had a strong influence on the magnetotail field configuration.

In addition to the modification of the existing tail current sheet in T96, a new tail current module is needed in order to model a transient, strongly tail-like geometry of the disturbed field at geosynchronous altitude [e.g., *Kokubun and McPherron*, 1981] while maintaining a positive B_z component in the central plasma sheet during the substorm growth phase. This additional current sheet is similar to the near-tail current sheet in T96, but its current density peaks around -6 R_E and has a much faster tailward falloff than that in T96. The shielding effect of the added tail current has also been taken into account in the new module.

To replicate the effect of the collapse of the nightside magnetic field, an empirical model of the substorm current wedge has recently been developed by *Tsyganenko* [1997], which consists of a pair of spread-out current loops that cross each other in the equatorial plane. Such a twin-loop topology mimics the wedge shape proposed by *McPherron et al.* [1973]. This wedge-shaped current circuit produces the dipolarization reconfiguration of the magnetic fields observed during the substorm expansion phase. The current wedge has adjustable longitudinal width and radial extension, along with an adjustable azimuthal shift away from the midnight meridian. The amplitude of the wedge current is also an adjustable parameter which controls the degree of the overall dipolarization.

The time-evolving magnetic field is modeled as follows. During the growth phase the tail current sheet thickness is assumed to decrease as a linear function of time, while the total tail current intensity (along with the corresponding shielding current) is increased linearly. The half thickness of the inner tail current sheet decreases from the initial value $D(X,Y)$ in the T96 model to a minimum value at the onset of the substorm expansion phase by multiplying a factor of $F(X)$:

$$F(X) = 1 - A \exp\left[-\left(\frac{X - X_c}{\Delta X}\right)^2\right] \qquad (1)$$

where X_c specifies the central thinning location in the X direction, ΔX is the scale size of the thinned region, and A is the factor by which the current sheet thickness is being reduced. At the same time, the tail current intensity is increased to $(1 + f_{\text{tail1}})$ times the T96 model value, and the added tail current intensity is increased from 0 at the beginning of the growth phase to an amplitude of f_{tail2} at the onset of the expansion phase. A similar localized thin current sheet was also applied in the model of *Pulkkinen et al.* [1991, 1992, 1994, 1998]. From the onset of the expansion phase until the end of the recovery phase, the thickness as well as the intensity of the tail current is gradually returned back to the T96 model values, and the added tail current gradually diminishes. In this time-evolving model, the intensity of the substorm wedge current f_{SCW} is controlled by the AL index. The magnetic field associated with the wedge current is turned on once the AL index falls below a specified threshold value AL_0:

$$f_{SCW} = 0 \qquad AL > AL_0$$

$$f_{SCW} = B(|AL| - |AL_0|) \qquad AL < AL_0 \qquad (2)$$

A longitudinal shift of the current wedge can also be introduced by rotating it with respect to the midnight meridian by an angle of θ.

We would like to point out that since both T96 and the modified magnetic field model consist of a set of modules, the region 1 and region 2 Birkeland currents as well as the substorm wedge currents are only approximately in the direction of an average B field when away from the low-altitude ionosphere [*Tsyganenko and Stern*, 1996; *Tsyganenko*, 1997].

3. Model-Observation Comparison

In this section, we demonstrate how the observed evolving magnetic field configurations are represented by the model. Our basic approach was to make a series of trial-and-correction tests, by comparing the predicted field variations with those measured by spacecraft during three isolated substorm events and by readjusting the model parameters. The final values of these variable parameters are listed in Table 1.

Table 1. Parameters Used for the Three Events

Parameters	January 9, 1997	January 12, 1997	May 15, 1996
A	0.99	0.97	0.93
X_c	7.0	7.3	7.5
ΔX	2.5	3.5	2.4
f_{tail1}	0.11	0.02	0.03
f_{tail2}	20	5	3
f_{SCW}	$0.8(\|AL\| - 120)$	$6.0(\|AL\| - 200)^{0.6}$	$0.5(\|AL\| - 80)$
$\theta*$	5°	12°	0°

*Positive θ represents a counterclockwise shift from the midnight meridian toward dawn.

3.1. Event 1: January 9, 1997

The solar wind and geomagnetic conditions for event 1 are shown in Figure 1. Figures 1a–1c are the 1-min averaged solar wind dynamic pressure and interplanetary magnetic field (IMF) measurements by the Wind satellite. At 0700 UT on January 9, 1997, Wind was located at (78, -60, -3) R_E in GSE (X, Y, Z) coordinates, and the average solar wind bulk speed was ~ 400 km/s. Thus a time delay of 21 min had been applied in Figure 1 to account for the solar wind propagation from the satellite location to the magnetopause. Since the purpose of this study is not the identification of the external trigger of the substorm, the accuracy in estimating the solar wind propagation time is not very critical. In Figure 1d, the solid lines show the auroral indices of AL and AU, respectively, which were derived from the 5-min averaged north-south component of the magnetic perturbations measured by 68 ground stations located in the auroral zone between |55°| and |76°| magnetic latitudes in all magnetic local times (MLTs). The dashed line, on the other hand, is the AL index but estimated from only those auroral stations located between 2100 and 0100 MLT. It therefore represents the westward auroral electrojet near the midnight sector. The good agreement between the solid and dashed AL curves indicates that the enhanced westward electrojets during the substorm were mainly confined in the midnight region. The midnight AL index began to decrease gradually at ~ 0600 UT and then dropped abruptly at ~ 0745 UT, marking the onset of the substorm expansion phase. After 0840 UT the substorm went into its recovery phase, as indicated by the gradual increase in AL. During the entire substorm interval the IMF remained nearly steady; there were some fluctuations in the solar wind dynamic pressure which may have caused the substorm (if the substorm was indeed externally triggered). The stable and small magnitude of the *Dst* index (not shown), with an average value of 2 nT, indicates that there were no magnetic storms during the period.

Figure 2 presents the comparison between the modeled magnetic fields and observations from the GOES 8 and 9 satellites. Both GOES 8 and 9 are geosynchronous satellites, and local midnight is at ~ 0500 UT for GOES 8 and 0900 UT for GOES 9. Starting at ~ 0600 UT, both satellites observed a gradual decrease in the B_z component, implying a growth of a tail-like magnetic field topology. However, as observed by both GOES 8 and 9, the tail-like stretching during the growth phase was not simply linear; rather, it evolved in two stages: a slow (with more than an hour in duration) stretching followed by a rapid (with 5–10 min in duration) stretching. This two-stage development of the

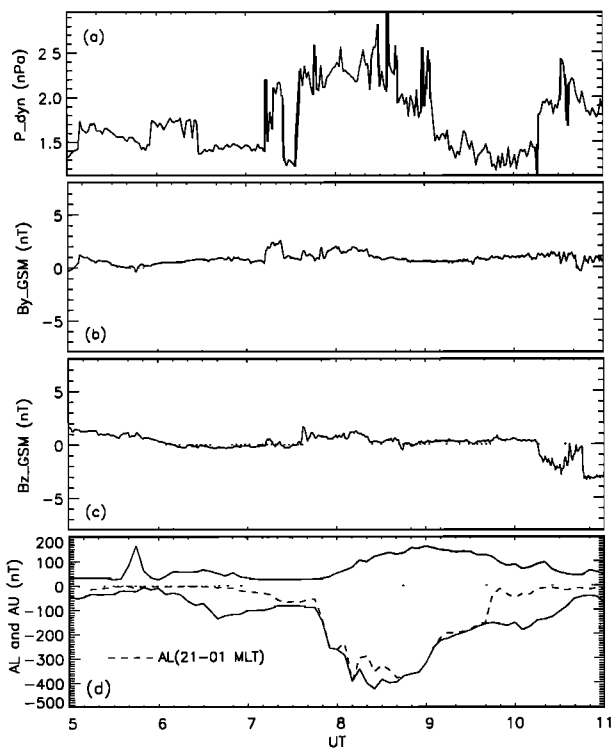

Figure 1. Solar wind and geomagnetic conditions between 0500 and 1000 UT on January 9, 1997: (a) solar wind dynamic pressure, (b) interplanetary magnetic field (IMF) B_y component, (c) IMF B_z component, and (d) AU and AL indices. A time delay of 21 min has been applied to the Wind data. IMF B_y and B_z components are in GSM coordinates.

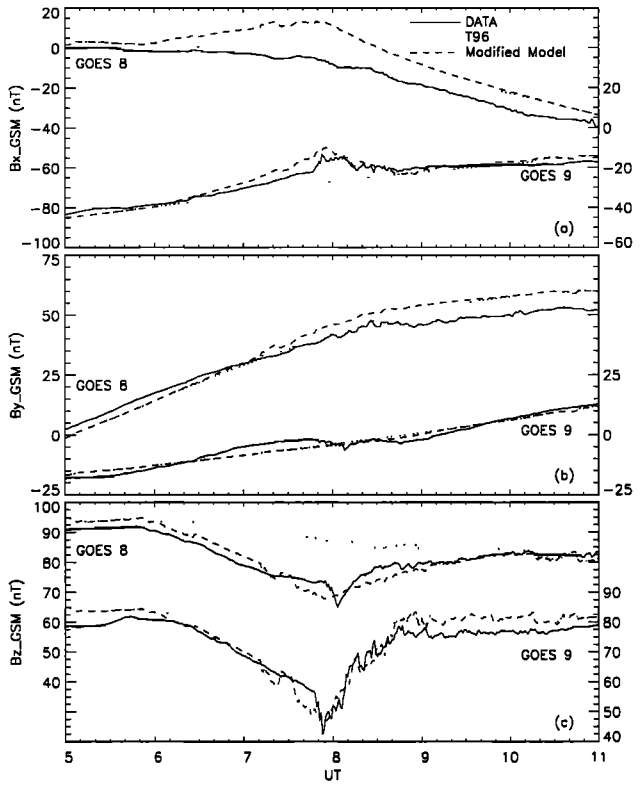

Figure 2. Comparison between the modeled and measured magnetic fields in GSM coordinates on January 9, 1997: (a) B_x component, (b) B_y component, and (c) B_z component. The scale for GOES 9 is given on the right side of Figures 2a–2c. The solid lines show the GOES data, the dotted lines show the T96 model values, and the dashed lines show the modified model results.

magnetic field configuration is similar to the schematic illustration of the tail current intensity change proposed by *Ohtani et al.* [1992a]. However, the explosive growth phase in their study was even shorter (less than 1 min) than the duration of the second stage of the rapid field stretching shown here. By 0753 UT, right before the field dipolarization, GOES 9 observed a total decrease in B_z of $\sim$ 35 nT. The dipolarization seen by GOES 8, however, was 9 min later at $\sim$ 0802 UT, and the total decrease in B_z for GOES 8 during the growth phase was $\sim$ 25 nT. Note that the dipolarization signature (e.g., the rapid increase in B_z) seen at the geosynchronous altitude was $\sim$ 8–17 min later than the substorm onset signature observed in the low-altitude ionosphere (e.g., the sudden decrease in the AL index). After 0900 UT both satellites measured a flattened B_z.

To model the magnetic field configuration during this substorm interval, the tail current amplitude parameters f_{tail1} and f_{tail2} were linearly increased from 0 at 0600 UT to the maximum values given in Table 1 at 0755 UT. At the same time, the current sheet thickness was reduced by 99% from the T96 model value. At present, because of the UT difference regarding the start time of the second explosive field stretching between the two GOES satellites, we have not incorporated the two-stage development of the tail current during the growth phase. Such a UT difference probably is caused by the motion of the tail current disruption that expands both azimuthally [*Nagai*, 1982; *Arnoldy and Moore*, 1983] and radially [*Lopez and Lui*, 1990; *Ohtani et al.*, 1991, 1992b]. In the future model improvements we shall include the tail current motion as an adjustable parameter so that the UT dependence of the local magnetic field configuration can be reproduced in the model. From 0755 to 1030 UT both f_{tail1} and f_{tail2} gradually returned to 0, and the thickness of the tail current sheet gradually resumed its T96 value. In this case, the substorm wedge current was activated at $\sim$ 0750 UT after the midnight AL index exceeded the threshold value of -120 nT. The current wedge was shifted 5° counterclockwise away from the midnight meridian plane.

As indicated by the dashed lines in Figure 2, the modified model shows a fairly good agreement with the GOES data, especially in the B_z component. The modified model reproduced quite well the decrease of B_z during the growth phase, the field dipolarization as indicated by the sharp rise in B_z during the expansion phase, and the relaxation in B_z during the late recovery phase. In contrast, the unmodified T96 model showed a nearly constant B_z throughout the substorm interval. However, at the GOES 8 location the modeled dipolarization appeared $\sim$ 7 min earlier than the observation. The time difference in dipolarization between the two GOES satellite indicates that the substorm-related disturbances, which are yet to be incorporated in the model, may propagate toward the Earth and/or expand azimuthally. For the B_x component the modified field resembled quite well the observed temporal variations, particularly for the GOES 9 data, but it overestimated the magnitude by 5–20 nT comparing with the GOES 8 data. As for the B_y component, both model results were similar to the GOES observations. Unfortunately, the Geotail satellite was located outside of the magnetosphere during this event.

3.2. Event 2: January 12, 1997

Figure 3 shows the 1-min averaged solar wind dynamic pressure and the IMF measured by the Wind satellite and the 5-min averaged AU and AL indices. A time delay of 22 min has been taken into account for the Wind data. As indicated by the AL index (both the solid and dashed AL lines), the growth phase of substorm began around 0630 UT, the onset of the substorm expansion phase was first observed at 0725 UT when AL started to decrease abruptly, and the recovery phase started at $\sim$ 0825 UT after AL reached its peak value of 1200 nT. There was also a second onset or intensification at $\sim$ 0810 UT when AL dropped sharply again after the first onset. In addition to the fluctuations in the solar wind dynamic pressure, there were large fluctuations in the IMF. *Dst* was nearly constant, with an average daily value of $\sim$ -16 nT.

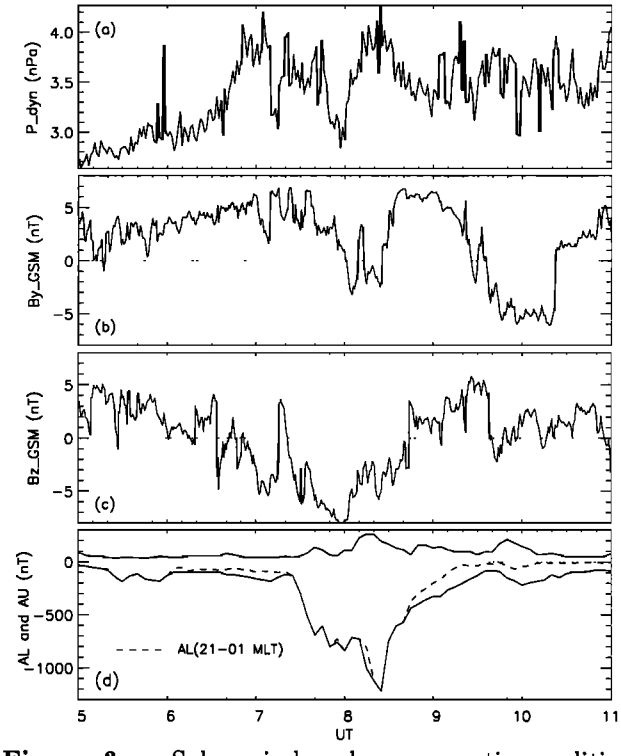

Figure 3. Solar wind and geomagnetic conditions between 0500 and 1000 UT on January 12, 1997: (a) solar wind dynamic pressure, (b) IMF B_y component, (c) IMF B_z component, and (d) AU and AL indices. The Wind data are lagged by 22 min. IMF B_y and B_z components are in GSM coordinates.

The GOES magnetic field observations are shown in Figure 4 as the solid lines. The clearest signature of dipolarization was seen at 0730 UT by GOES 9 and at 0740 UT by GOES 8. Again, the dipolarization at geosynchronous altitude was 5–15 min later than the ionospheric onset signature. It is worth pointing out that even though the magnitude of the AL index in this substorm event was about 3 times that for the January 9 substorm, the total observed reduction in B_z by the GOES satellites was $\sim$ 10 nT less than that in the previous case. Notice that the UT difference between the two substorm events was only $\sim$ 20 min.

In this case, the current sheet thickness was reduced by 97% from the T96 value at 0732 UT, and the maximal tail current amplitude was 0.02 for f_{tail1} and 5 for f_{tail2}. The substorm current wedge started to develop at $\sim$ 0728 UT when AL exceeded the threshold of -200 nT and was shifted 12° into the postmidnight sector. The intercomparison between the modeled magnetic fields and the GOES observations is shown in Figure 4. As one can see, the modified model again agreed reasonably well with the GOES observations. The modified model reproduced all main variations in the B_z component measured by the satellites, including the stretching of the magnetic field during the growth phase, the field dipolarization during the expansion phase, and the field relaxation during the recovery phase. The unmodified T96 model, on the other hand, totally failed to show any such changes associated with the substorm activity. Though the modified model showed the similar temporal B_x variations similar to the GOES 9 observations, it overestimated the field component by $\sim$ 10 nT. The overestimation was even larger when compared with the B_x and B_y measurements by GOES 8. We tried to incorporate a Y-dependent factor for the current sheet thickness in (1), similar to *Pulkkinen et al.* [1994, 1998]; however, the effect on B_x and B_y in this case was small. This indicates that a more complicated current sheet configuration probably is required in order to improve the agreement with the GOES 8 observations.

The Geotail satellite was located at about (-29, 6, -3) R_E in GSM coordinates at 0800 UT on January 12, 1997. Figure 5 shows the Geotail observations as well as the modeled magnetic fields. Figure 6 illustrates the X-Z projection of the magnetic field lines at the 0.8 MLT meridian. Figure 6a shows the unmodified T96 field lines, and Figure 6b shows the modified field lines. In both Figure 6a and Figure 6b the solid lines correspond to the field configuration at the onset of the substorm expansion phase, and the dotted lines correspond to the peak of the expansion phase. The modified model and the T96 model were nearly identical at the Geotail location, and both showed very small values, consistent

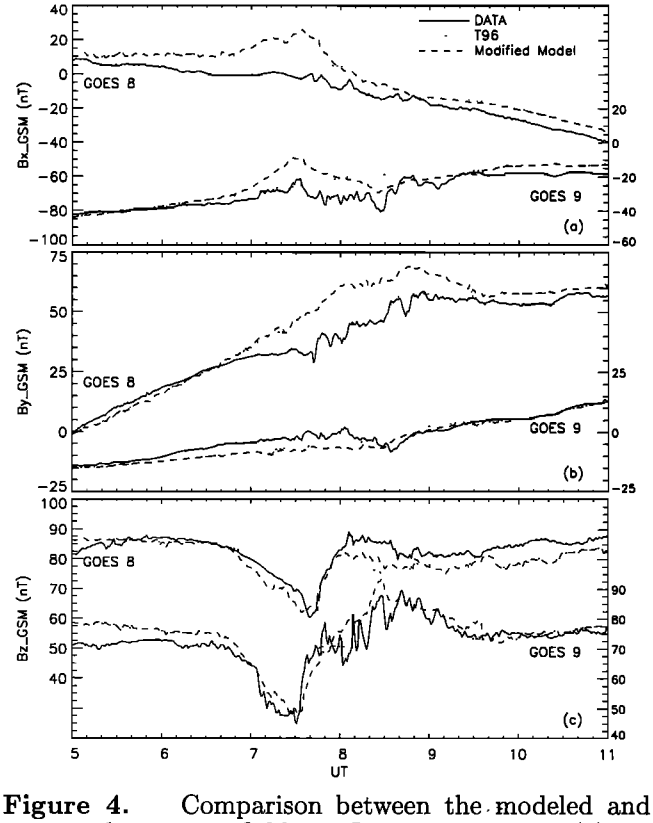

Figure 4. Comparison between the modeled and measured magnetic fields on January 12, 1997: (a) B_x component, (b) B_y component, and (c) B_z component. The scale for GOES 9 is given on the right side of Figures 4a–4c.

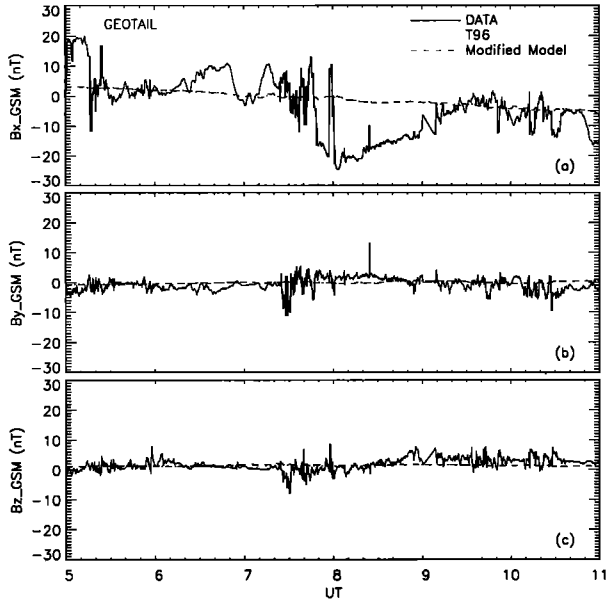

Figure 5. Comparison between the Geotail measurements and the modeled fields during January 12, 1997: (a) B_x component, (b) B_y component, and (c) B_z component. Note that the dotted and dashed lines are nearly overlapped.

with the B_y and B_z components measured by Geotail. For the B_x component, Geotail observed large field fluctuations between 0730 and 0800 UT, while the models showed a very small magnitude. However, as indicated in Figure 6, Geotail was located near the neutral sheet. So it is likely that the variations in the B_x component were due to the flapping motion of the magnetotail. On the basis of the model calculation, a fluctuation of ± 10 nT in B_x at the Geotail location ($X \sim$ -30 R_E) would correspond to a tail flapping of ± 1.5 R_E in the Z direction. This is consistent with the flapping motion observed by the ISEE spacecraft [*McComas et al.*, 1986]. A close examination of the Geotail data also showed that from 0748 to 0756 UT (between the two substorm onsets or intensification) the magnitude of B_x slowly increased from 17 to 20 nT, an indication of the magnetic field flux accumulation (or magnetic energy storage) in the tail lobe due to the effect of the second growth phase [*Baker et al.*, 1981; *Nagai et al.*, 1997]; from about 0805 to 0900 UT, Geotail was in the north lobe, and the gradual decrease in the magnetic field strength indicated a release of magnetic field flux (or magnetic energy dissipation) probably associated with magnetic reconnection [*Baker et al.*, 1981].

The January 12 event was a very intense substorm. Dramatic magnetic field dipolarization was evident when comparing the dotted lines in Figure 6b with those in Figure 6a. For instance, the dash-dotted line in both Figure 6a and Figure 6b has a footprint of 70° magnetic latitude in the northern ionosphere. In the unmodified T96 model, that ionospheric footprint would map to a midtail distance of X = -27 R_E; in the modified model, however, the same footprint maps much closer to the Earth at X = -7 R_E.

3.3. Event 3: May 15, 1996

Event 3 has been studied in detail by *Pulkkinen et al.* [1997, 1998]. Figure 7 shows the Wind observations (with a time delay of 14 min) of the solar wind dynamic pressure and the IMF B_y and B_z components as well as the auroral indices from 0050 to 0900 UT on May 15, 1996. By inspecting the AL index the substorm growth started at $\sim$ 0550 UT when the southward turning of the IMF B_z arrived at the magnetopause; the first onset of the substorm expansion phase was at $\sim$ 0625 UT, followed by a second onset at $\sim$ 0705 UT. There were no magnetic storms during this period, and the daily averaged Dst was -14 nT.

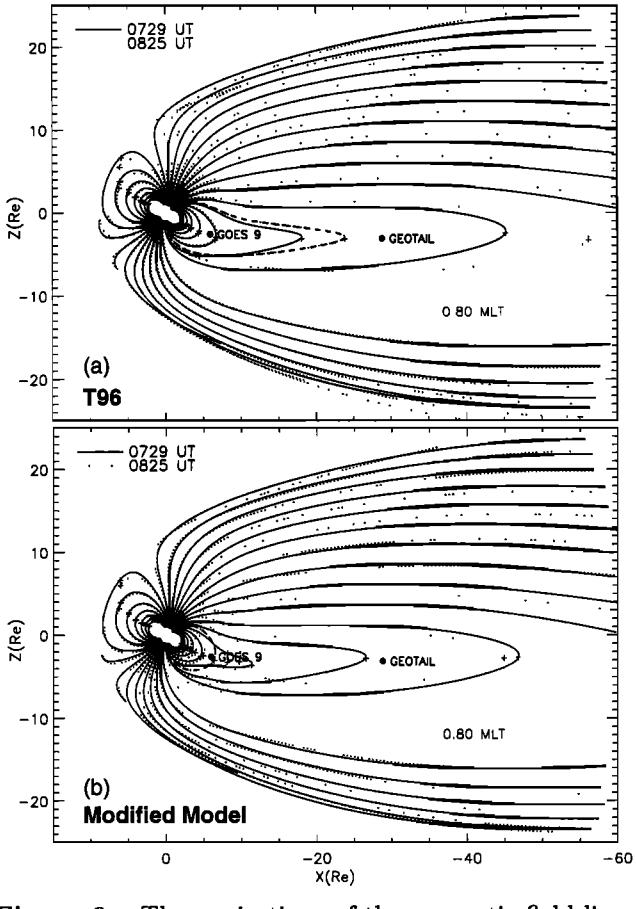

Figure 6. The projections of the magnetic field lines in the early morning meridian plane at 0.8 MLT for (a) the T96 model and (b) the modified model. The plus signs in Figures 6a and 6b indicate the equator as defined by the most distant point of the closed field line from the Earth. The dots indicate the satellite positions projected in the X-Z plane at 0800 UT. The two groups of solid and dotted field lines have the same ionospheric footprints that span from the north magnetic pole to 50° in magnetic latitude. The adjacent field lines are 3.33° apart, and the dash-dotted line has an ionospheric footprint at 70° in magnetic latitude. The dipole tilt angle in this case is about -28°.

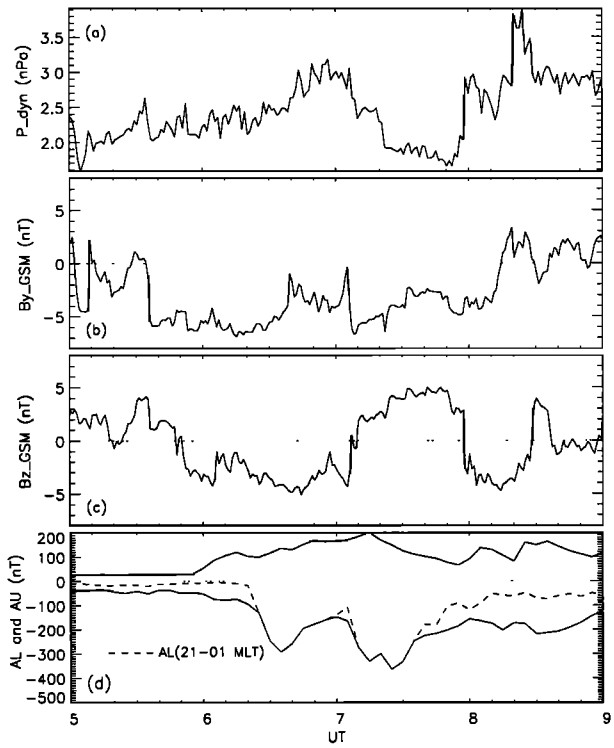

Figure 7. Solar wind and geomagnetic conditions between 0500 and 0900 UT on May 15, 1996: (a) solar wind dynamic pressure, (b) IMF B_y component, (c) IMF B_z component, and (d) AU and AL indices. A time delay of 14 min has been taken into account for the Wind data. IMF B_y and B_z components are in GSM coordinates.

In modeling the growth phase the current sheet thickness was thinned linearly in time by 93% from 0550 to 0625 UT, and the tail current amplitude was 0.03 (for f_{tail1}) and 3 (for f_{tail2}), respectively. From 0625 to 0757 UT, these adjustable parameters gradually returned to their initial values. The thin tail current sheet was centered at X_c = -7.5 R_E, close to the value (- 7.6 R_E) that *Pulkkinen et al.* [1998] used in their model.

Figure 8 shows the comparison between the modeled magnetic fields and the GOES and Geotail observations. At 0700 UT, GOES 8 was located at (-5.3, -3.2, 2.2) R_E, GOES 9 was located at (-5.4, 3.4, 1.5) R_E, and Geotail was located at (-7.4, -6.9, 0.2) R_E in GSM coordinates. Although the minimum AL value in this case was only 50 nT larger than that in the January 9 event, the total decrease in B_z observed by the three spacecraft during the growth phase was less than 20 nT. At the first onset at about 0625 UT, both GOES 8 and Geotail in the morning sector experienced a weak field dipolarization as indicated by the increase in B_z. However, the GOES 9 satellite located in the premidnight sector saw a further decrease in B_z, implying that the satellite was outside of the substorm wedge current. GOES 9 observed a dipolarization signature at 0655 UT (10 min before the second onset) as well as at 0712 UT (7 min after the second onset). After the second onset the B_z component at GOES 8 continued to decrease for another 17 min before increasing again at 0722 UT. The modified model showed a good agreement with the GOES 8 observations during the growth phase as well as at the first onset, but it failed to reproduce the time delay in dipolarization observed by GOES 8 during the second onset. Compared with the GOES 9 data, the modeled B_z field resembled the temporal variations during the second onset (the overestimate in magnitude was probably due to the fact that the base field represented by T96 was too high), but it failed to show the sharp decrease at the first onset. In order to simulate the complicated magnetic field configuration observed by both GOES satellites, it is necessary to include a time-dependent azimuthal shift of the substorm current wedge from the midnight meridian plane so that GOES 9 was located outside the wedge at the first onset and then came inside of the wedge during the second onset. Such an effort will be included in future model development. The bump-like structures near the two onsets in the B_y component at GOES 8 also indicated that the wedge currents should be more filamentary than that currently described in the model [*Tsyganenko*, 1997]. The agreement between the model and Geotail observations in all three field components was generally good.

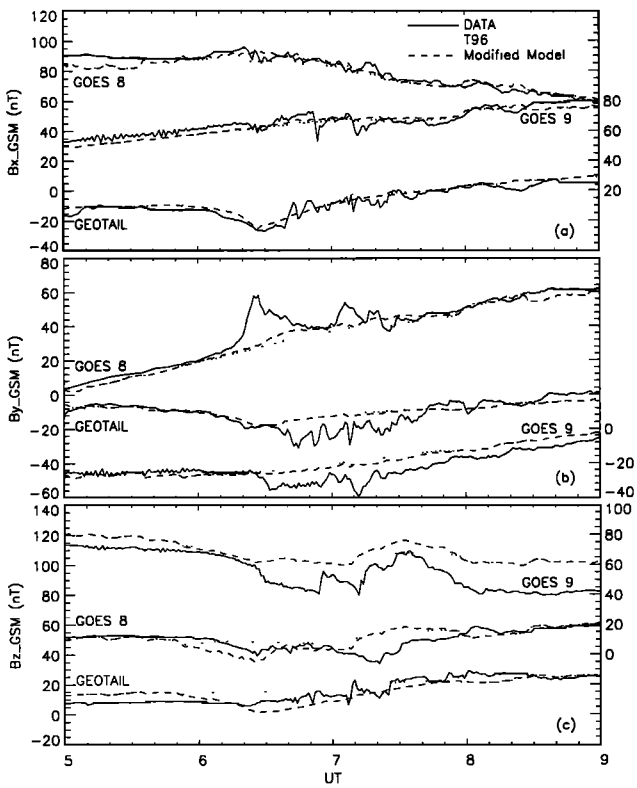

Figure 8. Comparison between the modeled and measured magnetic fields on May 15, 1996: (a) B_x component, (b) B_y component, and (c) B_z component. The scale for GOES 9 is again shown on the right side of Figures 8a–8c.

4. Discussion

Though they may differ in details from one substorm event to another, the general features of the central current sheet variations associated with substorms can be summarized as the following: During the growth phase the intensity of the tail current increases while its thickness decreases, causing a strong tailward stretching of the magnetic field lines. During the expansion phase the tail current disrupts in the near-Earth region, and the substorm wedge current develops, causing the magnetic field dipolarization. During the recovery phase the wedge current gradually disappears, and the tail current resumes its presubstorm configuration.

Our time-evolving substorm magnetic field model is based on the above observed features when modifying the T96 model. The parameter A listed in Table 1 corresponds to the maximum reduction of the central current sheet thickness at the onset. For the three substorm events studied the half thickness of the central current sheet was linearly decreased from 3 R_E at the beginning of the growth phase to 190 km (a 99% reduction) for January 9, 1997, 570 km (a 97% reduction) for January 12, 1997, and 1340 km (a 93% reduction) for May 15, 1996, respectively, at the onset of the expansion phase. The thinnest region was located between 7 and 7.5 R_E tailward of the Earth, as specified by the parameter X_c in Table 1. The half thickness of 190–1340 km is consistent with the previous observations of 0.1–0.3 R_E in the current sheet half thickness, but the central thinning location is earthward of the distance ($\sim$ 8–11 R_E) observed by satellites [*Fairfield*, 1984; *Sergeev et al.*, 1990, 1993; *Mitchell et al.*, 1990]. Note, however, that the thinning location X_c is a variable parameter. Because of the lack of satellite observations between 8 and 11 R_E during the three events studied, it is possible that the central thinning location was not being correctly defined in our model. On the other hand, since there are rarely observations available in the near-tail region between 7 and 8 R_E near the midnight meridian during substorms, a thin neutral sheet formed in this region may not be readily detectable. An enhanced current density in the near-Earth region due to both the tail current thinning and the added inner tail-disk current increasing is needed in order to reproduce the observed 30–40 nT reduction in B_z by the GOES satellites. This is similar to the effort made by *Kaufmann* [1987] and *Pulkkinen et al.* [1992, 1994, 1998] when modeling the stretched magnetic fields near geosynchronous altitude.

Observations have shown a wide range of variations of current density in the plasma-current sheet in the course of a substorm. On the basis of the observations made by a pair of closely spaced ISEE satellites, *Mitchell et al.* [1990] showed that the tail current sheet at the late growth phase was only $\sim$ 400 km (or $\sim$ 200 km in half thickness) at 11 R_E downstream of the Earth, with an inferred current density as high as 100 nA/m^2. By reanalyzing the same event, *Sergeev et al.* [1993] found that the half thickness of the current sheet changed from $\sim$ 3000 km at the beginning of the growth phase to $\sim$ 600 km 1 min before the onset, which was $\sim$ 3 times the value found by *Mitchell et al.* [1990]. Consequently, the current density of $\sim$ 35 nA/m^2 found by Sergeev et al. was about one third of that found by Mitchell et al.. Studies conducted by *Lui et al.* [1992] found a current density of 27–80 nA/m^2 near the Active Magnetospheric Particle Tracer Explorers (AMPTE)/CCE apogee ($\sim$ 8.8 R_E). However, smaller current densities in the central plasma sheet have also been reported. For example, *Sergeev et al.* [1994] found from the AMPTE/CCE measurements a magnetic field gradient of 80 nT/R_E, or an equivalent current density of $\sim$ 10 nA/m^2, at $\sim$ 8.5 R_E down the tail. Model simulations by *Pulkkinen et al.* [1994] showed a peak current density of 5–40 nA/m^2 in the central current sheet. Statistical study of *Nakai et al.* [1997] found that the neutral sheet current maximized near the geosynchronous altitude and that the maximal current density in the central current sheet during disturbed period (e.g., AL < -200 nT) was only $\sim$ 6 nA/m^2.

Changes of the tail current density in the course of substorms can be examined with Figure 9, which shows the profiles of the B_z component (Figure 9, top) and the dawn-to-dusk current density J_y (Figure 9, bottom) in the central current sheet for the three events. In each profile, the solid lines correspond to the beginning of the growth phase, the dotted lines correspond to the end of the growth phase (or the onset of the expansion phase), and the dashed lines correspond to the peak of the expansion phase. As the substorm growth phase proceeded, J_y gradually increased and reached the maximum value right before the onset of the expansion phase. The peak current density was located around 7 R_E tailward of the Earth. The maximum J_y value of 9–23 nA/m^2 is comparable with some of the previous results discussed above. During the expansion phase the westward tail current density gradually decreased, whereas an eastward current associated with the substorm current wedge increased around 12 R_E. For the intense substorm on January 12 the net tail current in the near-Earth region became eastward and was of a magnitude of 4.5 nA/m^2, which caused a negative B_z between 13 and 20 R_E. If the negative B_z structure was due to the formation of plasmoids, magnetic field reconnection should have occurred earthward of that region after the substorm onset. Unfortunately, there were no satellite observations available in the critical region between 8 and 29 R_E during that event. It is yet to be confirmed whether such a negative B_z structure was caused by magnetic reconnection so close to the Earth. Previous observations, however, have shown that magnetic reconnection usually takes place in the midtail region of 20–30 R_E [*Baumjohann et al.*, 1989; *Nagai et al.*, 1998; *Nagai and Machida*, 1998]. An alternative explanation for the negative B_z component is the

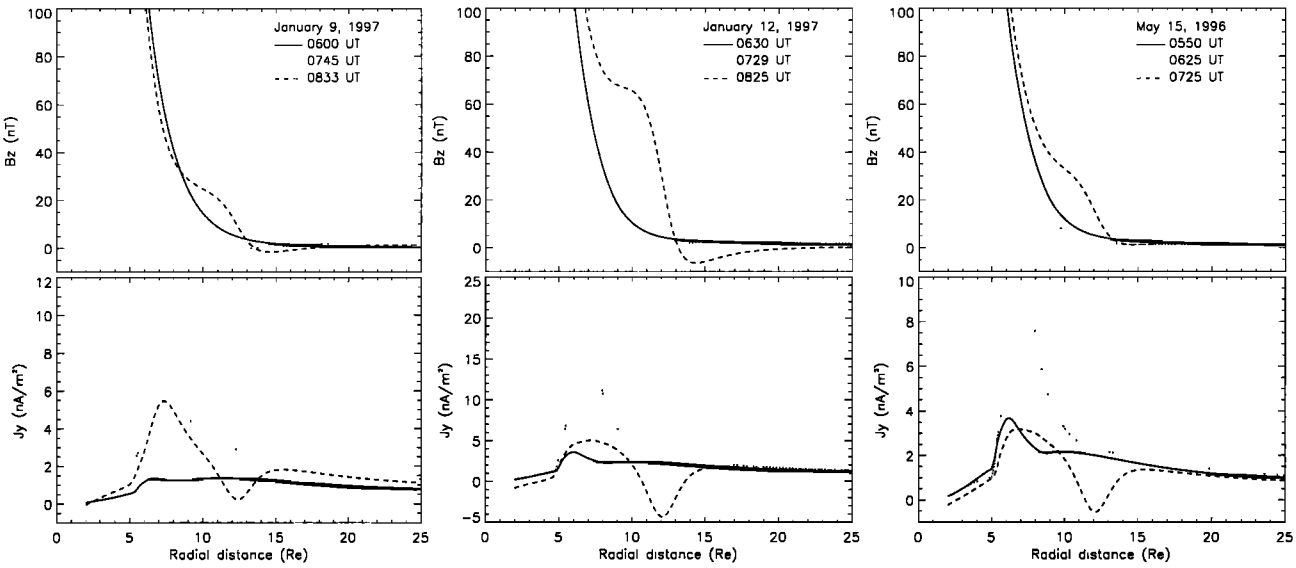

Figure 9. (top) The profiles of the GSM B_z component in the central current sheet at the beginning of the growth phase (solid lines), at the onset of the expansion phase (dotted lines), and at the peak of the expansion phase (dashed lines). (bottom) The distributions of the westward current density J_y in the central current sheet at the different substorm phases.

current disruption in the near-Earth region [*Lui*, 1996]. As pointed out by *Ohtani et al.* [1992b], the decrease in the tail current intensity can produce an X-type neutral line at the same location where the tail current disrupts. It is also interesting to note that the profiles of B_z and J_y shown in Figure 9 bear a striking resemblance to those shown in Figure 2 of *Birn and Hesse* [1996] from the MHD simulation, except that the peak of the eastward current in our model is located $\sim$ 15 R_E farther earthward than in their simulation.

The maximum amplitude of the wedge current f_{SCW}, listed in Table 1, was 208 for January 9, 379 for January 12, and 145 for May 15. Therefore the corresponding total wedge currents (f_{SCW} = 100 represents a total wedge current of 550 kA [*Tsyganenko*, 1997]) at the peak of the expansion phase were $\sim$ 1.1, 2.1, and 0.8 MA for these three events. These magnitudes are comparable with the integrated ionospheric field-aligned currents of region 1 sense in the midnight sector derived using the Assimilative Mapping of Ionospheric Electrodynamics (AMIE) procedure (the detailed AMIE results for these three events will be the subject of a separate paper).

5. Summary

As demonstrated in this paper, the performance of our time-evolving magnetic field model is rather encouraging. For the three substorms studied, the modified model showed reasonably good agreement with the GOES magnetic field observations, especially in the B_z component. The modified model reproduced quite well the tail-like magnetic field stretching during the growth phase, the dipolarization during the expansion, and the relaxation during the late recovery phase. In contrast, the unmodified T96 model showed a nearly constant B_z throughout the substorm intervals. However, a quantitative difference of 5–20 nT was found between the modeled and observed magnetic fields, particularly in the B_x component. The model is yet to be tested against observations beyond 8 R_E and should be refined in order to incorporate more complex configuration of the tail current sheet.

Our modeling effort confirmed the generally accepted scenario of substorms, including the formation of a thin current sheet during the growth phase and the disruption of the westward cross-tail current after the onset of the expansion phase associated with the development of the substorm current wedge. According to our model calculations, a thin current sheet of 190–1340 km in half thickness was formed in the near-tail region at $X \sim$ -7.5 R_E, and the maximum westward current density reached $\sim$ 9-23 nA/m^2. For the intense substorm event on January 12, 1997, a net eastward current flow was found between -11 and -13 R_E during the expansion phase, with a peak current density of 4.5 nA/m^2. The region of southward B_z tailward of X = -13 R_E was a result of a significant reduction of the dawn-to-dusk current in the near-tail model due to the formation of the substorm current wedge. Because of the lack of satellite observations in that region, it is not clear whether the formation of the X-type field geometry is a real feature or an artifact of the model.

Acknowledgments. The auroral indices used in this study were calculated from a worldwide network of ground magnetometer data, which were provided by T. Hughes at the Canadian Space Agency, L. Hakkinen at the Finnish Meteorological Institute, T. Moretto at the Danish Meteorological Institute, L. Morris at the National Geophysi-

cal Data Center of NOAA, K. Yumoto and the STEL at Nagoya University, G. van Beek of the Geological Survey of Canada, J. Posch at Augsburg College, D. Milling at the University of York, O. Troshichev at the Arctic and Antarctic Research Institute in Russia, K. Hayashi at the University of Tokyo in Japan, A. T. Weatherwax at the University of Maryland, G. Burns at the Atmospheric and Space Physics group at the Australian Antarctic Division, M. Pinnock at the British Antarctic Survey, V. Papitashvili at the University of Michigan, C. Maclennan at Bell Laboratories of Lucent Technologies, A. S. Potapov and S. I. Nechaev at the Institute of Solar-Terrestrial Physics at Irkutsk Observatory, and A. Zaitzev and V. Odintzov at IZMIRAN in Russia. The Wind magnetometer data were retrieved from the NASA CDAWeb database. Work at HAO/NCAR was supported in part by the NSF Space Weather program and by the NASA Space Plasma Theory and ISTP Guest Investigator programs. NAT acknowledges the support of the NASA ISTP GI Program (NASW-97024) and of the NSF Magnetospheric Physics Program (ATM-9501463). ATYL acknowledges the NSF support (ATM-9501544). G. Lu would like to thank M. Hesse, J. Birn, and D. Baker for helpful discussions.

Janet G. Luhmann thanks Michael Schulz and another referee for their assistance in evaluating this paper.

References

Arnoldy, R. L., and T. E. Moore, Longitudinal structure of substorm injections at synchronous orbit, *J. Geophys. Res., 88*, 3981, 1983.

Baker, D. N., E. W. Hones Jr., P. R. Higbie, R. D. Belian, and P. Stauning, Global properties of the magnetosphere during a substorm growth phase: A case study, *J. Geophys. Res., 86*, 8941, 1981.

Baumjohann, W., G. Pashmann, and C. A. Cattell, Average plasma properties in the central plasma sheet, *J. Geophys. Res., 94*, 6597, 1989.

Birn, J., and M. Hesse, Details of current disruption and diversion in simulations of magnetotail dynamics, *J. Geophys. Res., 101*, 15,345, 1996.

Fairfield, D. H., Magnetotail energy storage and the variability of the magnetotail current sheet, in *Magnetic Reconnection in Space and Laboratory Plasmas, Geophys. Monogr. Ser.*, vol. 30, edited by E. W. Hones Jr., pp. 168-177, AGU, Washington, D. C., 1984.

Kaufmann, R. L., Substorm currents: Growth phase and onset, *J. Geophys. Res., 92*, 7471, 1987.

Kokubun, S., and R. L. McPherron, Substorm signatures at synchronous altitude, *J. Geophys. Res., 86*, 11,265, 1981.

Lopez, R. E., and A. T. Y. Lui, A multisatellite case study of the expansion of a substorm current wedge in the near-Earth magnetotail, *J. Geophys. Res., 95*, 8009, 1990.

Lui, A. T. Y., Current disruption in the Earth's magnetosphere: Observations and models, *J. Geophys. Res., 101*, 13,067, 1996.

Lui, A. T. Y., R. E. Lopez, B. J. Anderson, K. Takahashi, L. J. Zanetti, R. W. McEntire, T. A. Potemra, D. M. Klumpar, E. M. Greene, and R. Strangeway, Current disruptions in the near-Earth neutral sheet region, *J. Geophys. Res., 97*, 1461, 1992.

McComas, D. J., C. T. Russell, R. C. Elphic, and S. J. Bame, The near-Earth cross-tail current sheet: Detailed ISEE 1 and 2 case studies, *J. Geophys. Res., 91*, 4287, 1986.

McPherron, R. L., C. T. Russell, and M. P. Aubry, Satellite studies of magnetospheric substorms on August 15, 1968, 9, Phenomenological model for substorms, *J. Geophys. Res., 78*, 3131, 1973.

Mitchell, D. G., D. J. Williams, C. Y. Huang, L. A. Frank, and C. T. Russell, Current carriers in the near-Earth cross-tail current sheet during substorm growth phase, *Geophys. Res. Lett., 17*, 583, 1990.

Nagai, T., Observed magnetic substorm signatures at geosynchronous altitude, *J. Geophys. Res., 87*, 4405, 1982.

Nagai, T., and S. Machida, Magnetic reconnection in the near-Earth magnetotail, in *New Perspective on the Earth's Magnetotail, Geophys. Monogr. Ser.*, vol. 105, edited by A. Nishida, D. N. Baker and S. W. H. Cowley, pp. 211-224, AGU, Washington, D. C., 1998.

Nagai, T., T. Mukai, T. Yamamoto, A. Nishida, S. Kokubun, and R. P. Lepping, Plasma sheet pressure changes during the substorm growth phase, *Geophys. Res. Lett., 24*, 963, 1997.

Nagai, T., M. Fujimoto, Y. Saito, S. Machida, T. Terasawa, R. Nakamura, T. Yamamoto, T. Mukai, A. Nishida, and S. Kokubun, Structure and dynamics of magnetic reconnection for substorm onsets with Geotail observations, *J. Geophys. Res., 103*, 4419, 1998.

Nakai, H., Y. Kamide, and C. T. Russell, Statistical nature of the magnetotail current in the near-Earth region, *J. Geophys. Res., 102*, 9573, 1997.

Ohtani, S., K. Takahashi, L. J. Zanetti, T. A. Potemra, R. W. McEntire, and T. Iijima, Tail current disruption in the geosynchronous region, in *Magnetospheric Substorms, Geophys. Monogr. Ser.*, vol. 64, edited by J. R. Kan et al., pp. 131-137, AGU, Washington, D. C., 1991.

Ohtani, S., K. Takahashi, L. J. Zanetti, R. W. McEntire, and T. Iijima, Initial signatures of magnetic field and energetic particle fluxes at tail reconnection: Explosive growth phase, *J. Geophys. Res., 97*, 19,311, 1992a.

Ohtani, S., S. Kokubun, C. T. Russell, Radial expansion of the tail current disruption during substorms: A new approach to the substorm onset region, *J. Geophys. Res., 97*, 3129, 1992b.

Pulkkinen, T. I., et al., Modeling the growth phase of a substorm using the Tsyganenko model and multi-spacecraft observations: CDAW-9, *Geophys. Res. Lett., 18*, 1963, 1991.

Pulkkinen, T. I., D. N. Baker, R. J. Pellinen, J. Buchner, H. E. J. Koskinen, R. E. Lopez, R. L. Dyson, and L. A. Frank, Particle scattering and current sheet stability in the geomagnetic tail during the substorm growth phase, *J. Geophys. Res., 97*, 19,283, 1992.

Pulkkinen, T. I., D. N. Baker, P. K. Toivanen, R. J. Pellinen, R. H. W. Friedel, and A. Korth, Magnetospheric field and current distributions during the substorm recovery phase, *J. Geophys. Res., 99*, 10,955, 1994.

Pulkkinen, T. I., D. N. Baker, R. J. Pellinen, J. S. Murphree, and L. A. Frank, Mapping of the auroral oval and individual arcs during substorms, *J. Geophys. Res., 100*, 21,987, 1995.

Pulkkinen, T. I., et al., Solar wind-magnetosphere coupling during an isolated substorm event: A multispacecraft ISTP study, *Geophys. Res. Lett., 24*, 983, 1997.

Pulkkinen, T. I., et al., Two substorm intensifications compared: Onset, expansion, and global consequences, *J. Geophys. Res., 103*, 15, 1998.

Sergeev, V. A., P. Tanskanen, A. Korth, and R. C. Elphic, Current sheet thickness in the near-Earth plasma sheet during substorm growth phase, *J. Geophys. Res., 95*, 3819, 1990.

Sergeev, V. A., D. G. Mitchell, C. T. Russell, and D. J. Williams, Structure of the tail plasma/current sheet at $\sim 11\ R_E$ and its changes in the course of a substorm, *J. Geophys. Res., 98*, 17,345, 1993.

Sergeev, V. A., T. I. Pulkkinen, R. J. Pellinen, and N. A. Tsyganenko, Hybrid state of the tail magnetic configuration during steady convection events, *J. Geophys. Res., 99*, 23,571, 1994.

Slavin, J. A., et al., An ISEE 3 study of average and substorm conditions in the distant magnetotail, *J. Geophys. Res., 90*, 10,875, 1985.

Tsyganenko, N. A., Global quantitative models of geomagnetic field in the cislunar magnetosphere for different disturbance levels, *Planet. Space Sci., 35*, 1347, 1987.

Tsyganenko, N. A., A magnetospheric magnetic field model with a warped tail current sheet, *Planet. Space Sci., 37*, 5, 1989.

Tsyganenko, N. A., Modeling the Earth's magnetospheric magnetic field confined within realistic magnetopause, *J. Geophys. Res., 100*, 5599, 1995.

Tsyganenko, N. A., Effects of the solar wind conditions on the global magnetospheric configuration as deduced from data-based field models, in *Proceedings of the ICS-3 Conference, Versailles, France, May 12-17, 1996, Eur. Space Agency Spec. Publ., ESA SP-389*, 181-185, 1996.

Tsyganenko, N. A., An empirical model of the substorm current wedge, *J. Geophys. Res., 102*, 19,935, 1997.

Tsyganenko, N. A., and M. Peredo, Analytical models of the magnetic field of disk-shaped current sheets, *J. Geophys. Res., 99*, 199, 1994.

Tsyganenko, N. A., and D. P. Stern, Modeling the global magnetic field of the large-scale Birkeland current systems, *J. Geophys. Res., 101*, 27,187, 1996.

Yamamoto, T., K. Shiokawa, and S. Kokubun, Magnetic field structures of the magnetotail as observed by Geotail, *Geophys. Res. Lett., 21*, 2875, 1994.

S. Kokubun, Solar-Terrestrial Environment Laboratory, Nagoya University, Nagoya 464-01, Japan.

G. Lu, High Altitude Observatory, National Center for Atmospheric Research, 3540 Mitchell Lane, Boulder, CO 80301. (ganglu@ ucar.edu)

A. T. Y. Lui, Applied Physics Laboratory, Johns Hopkins University, Laurel, MD 20723-6099.

T. Nagai, Tokyo Institute of Technology, Ookayama 2-12-1 Meguro, Tokyo 152-8551, Japan.

H. J. Singer, Space Environment Center, National Oceanic and Atmospheric Administration, 325 Broadway, Boulder, CO 80303.

N. A. Tsyganenko, NASA Goddard Space Flight Center, Greenbelt, MD 20771.

(Received September 28, 1998; revised February 2, 1999; accepted March 12, 1999.)